BACKUP ATTITUDE CONTROL ALGORITHMS FOR THE MAP SPACECRAFT

James R. O'Donnell, Jr., Ph.D.[1], Stephen F. Andrews[1],
Aprille J. Ericsson-Jackson, Ph.D.[1], Thomas W. Flatley, Ph.D.[1],
David K. Ward[2], P. Michael Bay[3]
Goddard Space Flight Center
Greenbelt, MD 20771 USA

The Microwave Anisotropy Probe (MAP) is a follow-on to the Differential Microwave Radiometer (DMR) instrument on the Cosmic Background Explorer (COBE) spacecraft. The MAP spacecraft will perform its mission, studying the early origins of the universe, in a Lissajous orbit around the Earth-Sun L_2 Lagrange point. Due to limited mass, power, and financial resources, a traditional reliability concept involving fully redundant components was not feasible. This paper will discuss the redundancy philosophy used on MAP, describe the hardware redundancy selected (and why), and present backup modes and algorithms that were designed in lieu of additional hardware redundancy to improve the odds of mission success. Three of these modes have been implemented in the spacecraft flight software. The first onboard mode allows the MAP Kalman Filter to be used with digital sun sensor (DSS) derived rates, in case of the failure of one of MAP's two two-axis inertial reference units. Similarly, the second onboard mode allows a "star tracker only" mode, using attitude and derived rate from one or both of MAP's star trackers for onboard attitude determination and control. The last backup mode onboard allows a sun-line angle offset to be commanded which will allow solar radiation pressure to be used for momentum management and orbit stationkeeping. In addition to the backup modes implemented on the spacecraft, two backup algorithms have been developed in the event of less likely contingencies. One of these is an algorithm for implementing an alternative scan pattern to MAP's nominal dual-spin science mode using only one or two reaction wheels and thrusters. Finally, an algorithm has been developed that uses thruster "one-shots" while in science mode for momentum management. This algorithm has been developed in case system momentum builds up faster than anticipated, to allow adequate momentum management while minimizing interruptions to science. In this paper, each mode and algorithm will be discussed, and simulation results presented.

SYSTEM ENGINEERING

The Microwave Anisotropy Probe (MAP) spacecraft, shown in Figure 1, is the second of a series of Medium Explorer, or MIDEX missions (ref. 1). The MIDEX program was designed as an intermediate option between the Explorer Program's full-sized missions and Small Explorer (SMEX) spacecraft. Each class of spacecraft follows a different redundancy philosophy; the full-sized Explorers maximize reliability by implementing fully redundant spacecraft, while the SMEX missions minimize cost by only allowing single-string components. The MIDEX goal is

[1] Flight Dynamics Analysis Branch, Code 572
[2] Systems Engineering Branch, Code 571
[3] Jackson and Tull

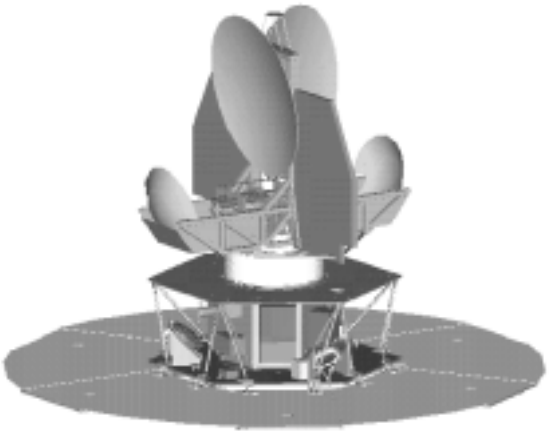

Figure 1: The MAP Spacecraft

to use redundancy intelligently, in order to get the "best bang for the buck", consistent with its mandate of offering the best mission under a fixed cost cap. In many ways, the MIDEX philosophy is the most difficult of the three (Explorer, MIDEX, and SMEX) to follow. There are no set rules for what redundancy should be present, so a decision must be made for each spacecraft element.

MAP's Redundancy Philosophy

During the initial system engineering of the MAP spacecraft, and at a few other occasions during the lifetime of the mission (e.g., as a result of points raised at MAP's Confirmation Review), decisions were made as to what redundancy to include, and how to implement it. These decisions were made according to the following redundancy selection criteria:

- The overall results of the failure likelihood of a hardware component based on a historical database and independent Probability of Success (Ps) calculations was considered.
- Resource impacts of redundant component cost, mass, and power) were considered.
- It was determined whether or not the redundancy, be it hardware or software, was modular (able to be added or removed with minimal impacts to the existing spacecraft design).
- For potential redundant hardware, the availability of "algorithmic redundancy" (such as the algorithms described later in this paper) was taken into account.
- Conversely, the ability of an additional component to backup multiple components was *also* taken into account.

MAP Redundancy: Components and Algorithms

As a result of the redundancy philosophy detailed above, the following components were selected to have hardware backups. Another transponder was added, based on the failure probability from a historical database. Two thrusters were added to the design, due to the criticality of perigee burns and the relatively low cost, mass, and power impacts from the added thrusters. Because the star tracker used on MAP was a complex piece of new technology critical to the success of the mission, a redundant tracker was added. Also, the fact that adding an addition tracker of the same type would be a small modular change to the design, and that both trackers could serve as backup rate sources to the inertial reference units (IRU) made it a good choice for hardware redundancy. A redundant main processor and interface electronics box was added, also because of the complex new technology of the processor used. Finally, an additional set of coarse sun sensors (CSS) was added; there were no concerns about the existing CSSs, but adding a new set was simpler than cross-strapping one set to both interface electronics boxes.

A number of components were not selected for hardware redundancy, even though they appeared high on the historical database of potential failure items. A fourth reaction wheel assembly (RWA) was not added because of mass and power limitations, as well as the existence of a possible backup algorithm (which is described later in this paper). A third two-axis IRU, which would provide full redundancy in all three axes, was not added, primarily because of the existence of DSS and star tracker backup algorithms. Redundant power system electronics (PSE) was not added because the existing design was robust enough to survive many failures using existing electronics. Finally, the science instrument itself already possessed some capability for graceful degradation of performance, so it was determined that nothing additional was needed.

One component was included on the MAP spacecraft even though, strictly speaking, it was not needed at all, in seeming violation of the "intelligent redundancy" philosophy. The DSS was not needed for any nominal mission mode. It was included on the spacecraft—in fact, a second DSS head was added well after the initial design—because of several factors. The DSS unit is very reliable, and can act as a backup to the two IRU axes which are not already redundant. With nominal mission attitudes, information from the DSS is always available; the second DSS head added allows the unit to be used as a backup rate source during the entire perigee pass (during which MAP must thrust along its own velocity vector). This became important when concerns were raised about poor star tracker performance in the Van Allen radiation belts.

ON-BOARD BACKUP ALGORITHMS FOR MAP

The development of backup attitude control algorithms for the MAP spacecraft, and the decision of which to implement on-board and which to keep in reserve (not implemented but available in the event of in-flight failures), was dictated by the redundancy philosophy described in the previous section. In general, those algorithms were placed on-board that were easy to implement and/or provided a backup to a more likely failure item.

Three algorithms of this nature were implemented on MAP. The first allows the on-board Kalman Filter to be run with a DSS-derived rate in place of an IRU rate. The second uses the attitude quaternion and a derived rate from MAP's star tracker(s) to be used in place of both IRU rates and propagated attitude. Finally, a means of establishing a bias attitude command with respect to the sun line was implemented; this bias would be used in an algorithm for providing orbit and momentum management using solar radiation pressure.

Kalman Filter w/DSS Rate

Nominally, the MAP on-board Kalman Filter uses two two-axis IRUs to provide three axes of rate information, and updates the propagated attitude and the gyro drift bias corrections based on star tracker attitude quaternions and DSS sun vector measurements. In the event of the failure of one of the IRUs, an alternate rate source for either the x or y axis is needed. In this case, it is possible to substitute a DSS-derived rate for the missing IRU axis, and to continue to run the Kalman Filter, updating the attitude and gyro bias with star tracker measurements only.

DSS Rate Algorithm

The data from the DSS can be used to compute the body rates about the x and y spacecraft axes. The DSS output is the measured sun vector in the body frame. Given $\hat{s}$, the unit vector to the sun in the body-fixed frame, and $\vec{\omega}$, the body rate, the rate of change of $\hat{s}$ is:

$$\dot{\hat{s}} = -\vec{\omega} \times \hat{s} = \hat{s} \times \vec{\omega}$$

In component form, this can be written as:

$$\dot{s}_x = s_y \omega_z - s_z \omega_y$$
$$\dot{s}_y = s_z \omega_x - s_x \omega_z$$
$$\dot{s}_z = s_x \omega_y - s_y \omega_x$$

In the event of a single IRU failure, the body z-axis rate will still be known, because each IRU has one measurement axis in that body axis. With ω_z known, ω_x and ω_y can be found from the DSS measurement by solving the first two component equations for the unknown body rates:

$$\omega_x = (\dot{s}_y + s_x \omega_z) / s_z$$
$$\omega_y = (-\dot{s}_x + s_y \omega_z) / s_z$$

Since the IRU measures the average rate over the previous control cycle, the DSS data must be averaged also, or there will be a half-cycle (0.5 second) offset between the rate that ω_z represents, and the sun vector that s_x and s_y represent. At low rates, this is not a problem, but at the nearly 3°/sec MAP fast spin rate, this half-cycle offset is too large to ignore. Thus, the sun vector used in the above equations must be the average sun vector in the cycle over which the DSS rate (and IRU rate) is calculated:

$$s_x = 0.5(s_x(k) + s_x(k-1))$$
$$s_y = 0.5(s_y(k) + s_y(k-1))$$

where k indicates the current cycle, and $k-1$ is the previous cycle. In addition, the sun vector rate must also be the average rate of change of the sun vector over the control cycle:

$$\dot{s}_x = (s_x(k) - s_x(k-1)) / \Delta t_{DSS}$$
$$\dot{s}_y = (s_y(k) - s_y(k-1)) / \Delta t_{DSS}$$

where Δt_{DSS} is the time between DSS samples.

The end result is the DSS measurement of the x and y axis body rates. Both of these rates are calculated each control cycle and telemetered to the ground, and are available to be used in the Kalman Filter. Nominally, the DSS rates are also used in a system rate check that compares the IRU rates, DSS rates, and AST rates to each other.

Kalman Filter Adjustments for DSS Rates

There were two ways that the DSS-derived body rate could be used to replace the IRU rate in the Kalman Filter. First, the state equations and noise models could be redesigned to incorporate the different rate source, and that model would be used only when the filter was configured to use the DSS. Second, the DSS rate could be treated as if it came from an IRU, with a parameter change to the existing Kalman Filter model. Software impacts and schedule considerations led to the choice of option two. During testing, or in the event of an IRU failure on-orbit, the Kalman Filter is configured to use a DSS rate, and the appropriate parameters are adjusted to account for the different statistical qualities of the DSS rate compared to the IRU rate. Although the DSS rate is correlated in time through the calculation of the average sun vector, each DSS-derived rate was treated as if it were uncorrelated. In addition, since the DSS output is a position measurement, there is no drift associated with it, as with an IRU measurement. For these reasons, the standard deviation of the IRU rate random walk (σ_u) was reduced by half to model the decreased drift characteristics of the DSS rate measurement. In addition, since a noisy DSS measurement was being differentiated to generate the DSS rate, this rate would have higher white noise than the IRU rate. Thus, the rate white noise standard deviation (σ_v) was increased by an order of magnitude over the nominal IRU model. Finally, the DSS was disabled as a filter update sensor.

Simulation Results

Figure 2 and Figure 3 show, respectively, MAP's simulated IRU-measured x- and y-axis body rates and the Observing Mode performance (precession and spin rates and sun line angle) when in its nominal configuration. Figure 4 shows what the corresponding DSS-derived x- and y-axis body rates look like. As expected, they are much noisier. (Note that the MAP flight software was designed with the capability to filter both the DSS- and AST-derived rates, though no filter has currently been put in place for either.) Figure 5 shows the simulated Observing Mode performance when the DSS x-axis body rate is used in the on-board Kalman Filter.

Unsurprisingly, the Observing Mode performance in the backup DSS rate mode is noticeably degraded from the nominal case. However, both the sun line angle and spin rate are well within their respective specifications of $22.5 \pm 0.25°$ and $2.784°/\text{sec} \pm 5\%$. The precession rate requirement of $0.1°/\text{sec} \pm 5\%$ is violated in this backup mode, though degraded performance would be acceptable in this case. It is possible that a DSS rate filter would improve these results.

AST-Only for Attitude and Rates

Because the star trackers selected to be used on the MAP spacecraft are quaternion-output trackers, it is a fairly straightforward process to derived rates in each body axis from successive attitude quaternions. If the attitude quaternion at a given time k is denoted q_k, then the Δquaternion from one cycle to the next can be calculated as $\Delta q = q_{k-1}^{-1} \otimes q_k$, where $\otimes$ denotes quaternion multiplication. Since Δq can be expressed as the Euler axis and angle parameters $[e_1 \sin(\Delta\phi/2), e_2 \sin(\Delta\phi/2), e_3 \sin(\Delta\phi/2), \cos(\Delta\phi/2)]$, the derived rates can be found using the relationship $\omega = [e_1 \Delta\phi/\Delta t, e_2 \Delta\phi/\Delta t, e_3 \Delta\phi/\Delta t]$.

Figure 2: Nominal IRU Body Rates

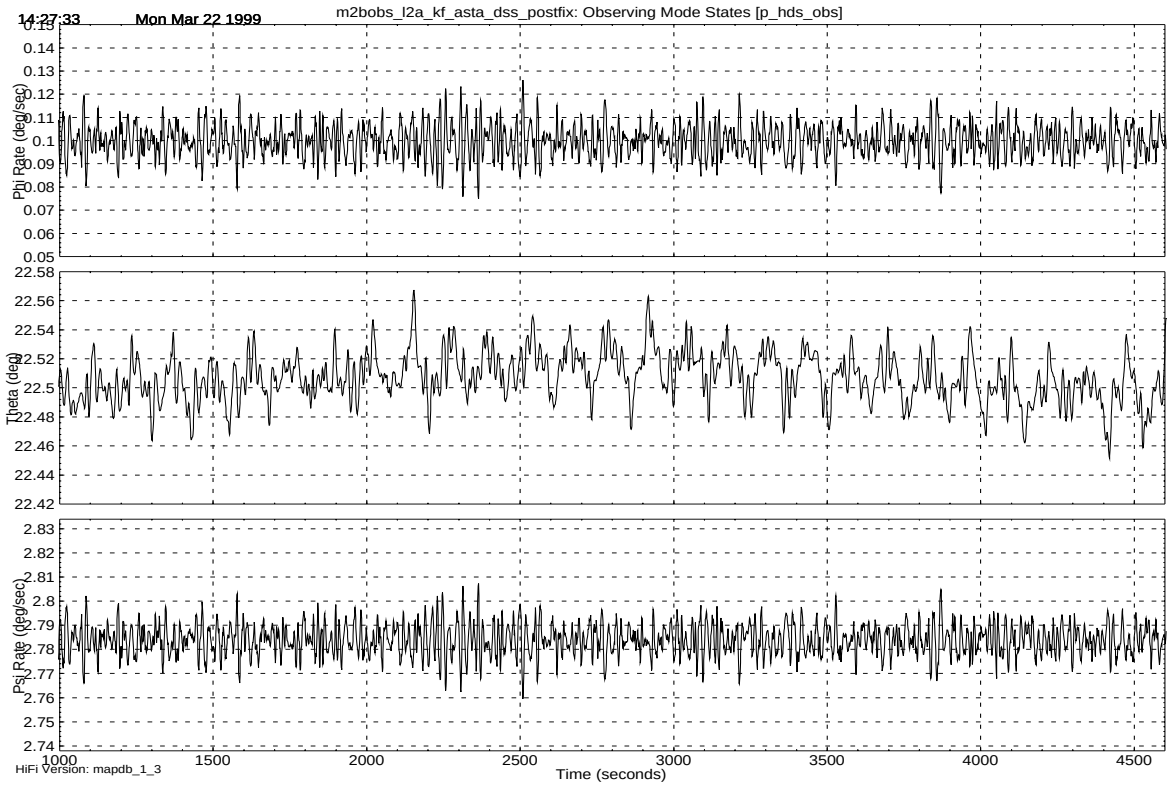

Figure 3: Nominal Observing Mode Performance

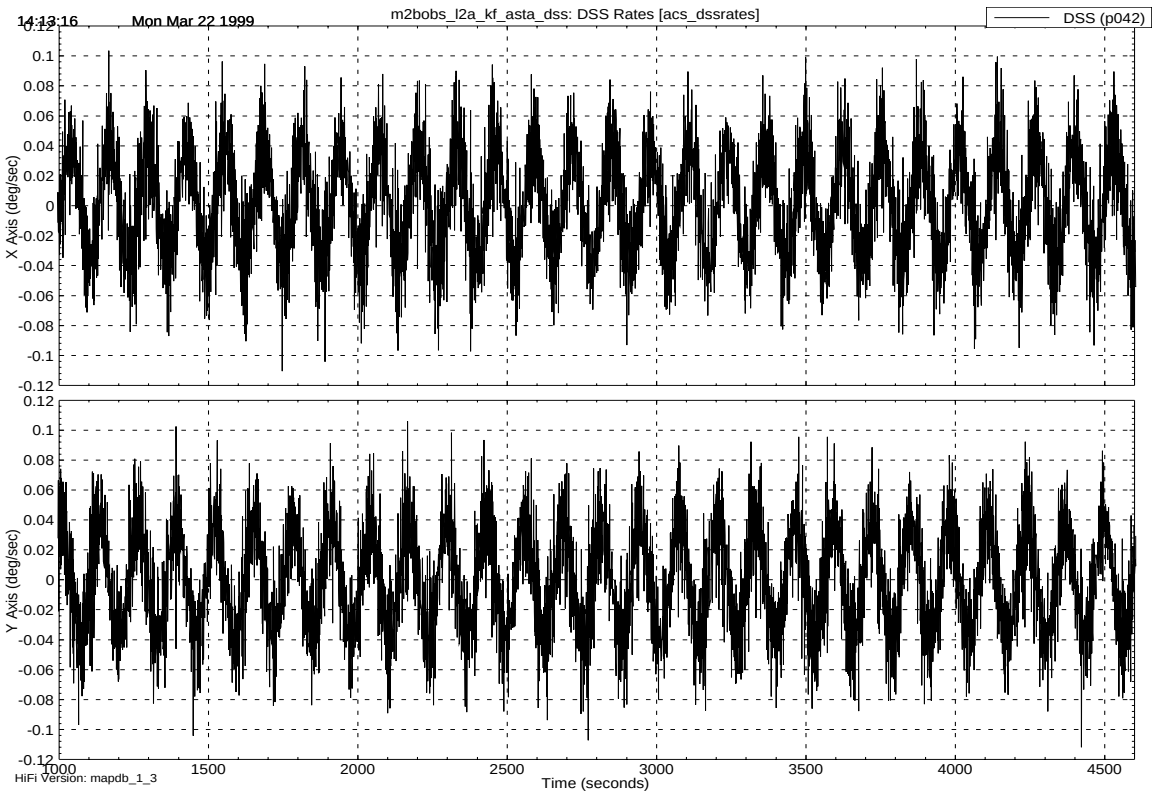

Figure 4: DSS-Derived Body Rates

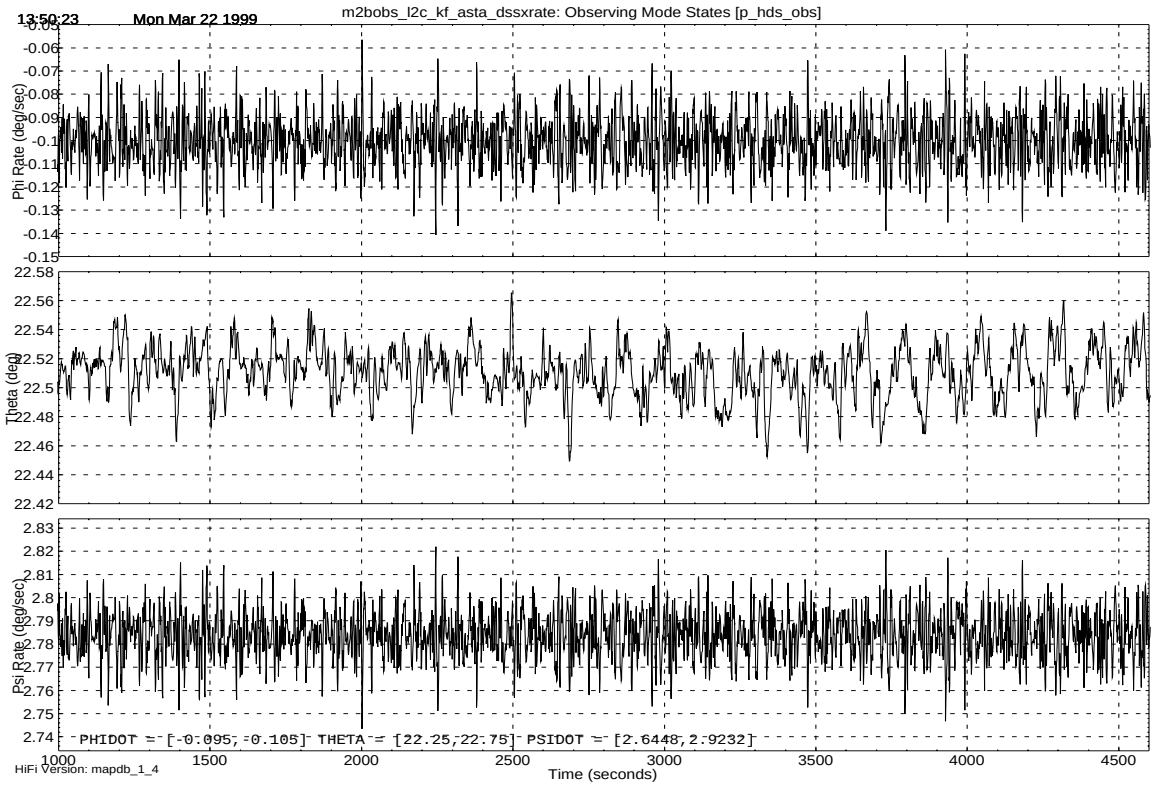

Figure 5: Observing Mode Performance Using DSS-Derived Rate in Kalman Filter

Figure 6 shows star tracker derived x- and y-axis body rates (the z-axis rate shows similar characteristics; only x and y are shown here to make it easier to compare with the IRU and DSS rates shown in Figure 2 and Figure 4). Figure 7 shows the Observing Mode performance using star tracker attitude and derived rates. As with DSS rate backup algorithm, the performance of the system in Observing Mode using the star tracker backup algorithm satisfies the sun line angle and spin rate requirement, but not the precession rate requirement. It is also interesting to note that, while the star tracker derived rates appear to be a bit better than those from the DSS, the Observing Mode performance is slightly better with the DSS rate backup. This is because of the action of the Kalman Filter, which can still be used in the DSS case.

Sun Line Bias Algorithm

Solar Radiation Pressure (SRP) will be the main perturbation to the MAP spacecraft orbits when it is in the vicinity of the Earth-Sun L_2 Lagrange point. The two main effects of a the SRP on MAP will be to shift the center of its orbit about the L_2 point, and also to cause a buildup of spacecraft system momentum. It is nominally planned to conduct orbit and momentum maintenance operations with the spacecraft four times a year.

Tene, et. al., have proposed a means by which, using small variations in the orientation of MAP's sun shield as it spins and cones about the sun line in its Observing Mode, it might be possible to use the SRP to reduce or even eliminate the need to conduct thruster operations for the purpose of orbit maintenance (ref. 2). Because of the sensitivity of the MAP orbit about L_2, small accelerations are capable of either causing or preventing the spacecraft to escape from the vicinity of L_2.

The average acceleration imparted on MAP due to the SRP was estimated to be 0.2 $\mu m/sec^2$. Since the spin axis of the MAP spacecraft precesses about the sun line every hour, the average SRP acceleration is directed away from the sun. If the precession axis points exactly at the sun and the precession motion is symmetric, there would be no acceleration perpendicular to this axis. Any bias in the precession axis would cause a perpendicular acceleration to the sun line; it is this acceleration that Tene proposes could be used for orbit maintenance. During Observing Mode, MAP's spin axis must be precessed about the sun line at an angle of $22.5 \pm 0.25°$. Given the nominal expected performance of the Observing Mode controller, an offset as high as 0.1° could be applied and still allow science requirements to be met. Tene showed that with such an offset, an average acceleration can be applied perpendicular to the sun line on the order of 0.5 nm/sec^2. With the correct bias, this acceleration can help MAP maintain a desired orbit.

Tene originally proposed an onboard controller that would take attitude and orbit information to autonomously determine the sun line bias to be applied. Subsequently, it was determined that the necessary bias changes slowly enough (on the order of a week or more) that it could be very simply implemented as a constant sun line bias, expressed as a quaternion rotation about MAP's rotating sun reference (RSR) frame, that could be commanded by the ground. This bias would rotate the entire RSR frame; the Observing Mode Euler angles and rates would remain unchanged. However, the bias would show up in the sun angle. Figure 8 shows the effects of a 0.1° sun line bias commanded at 500 sec.

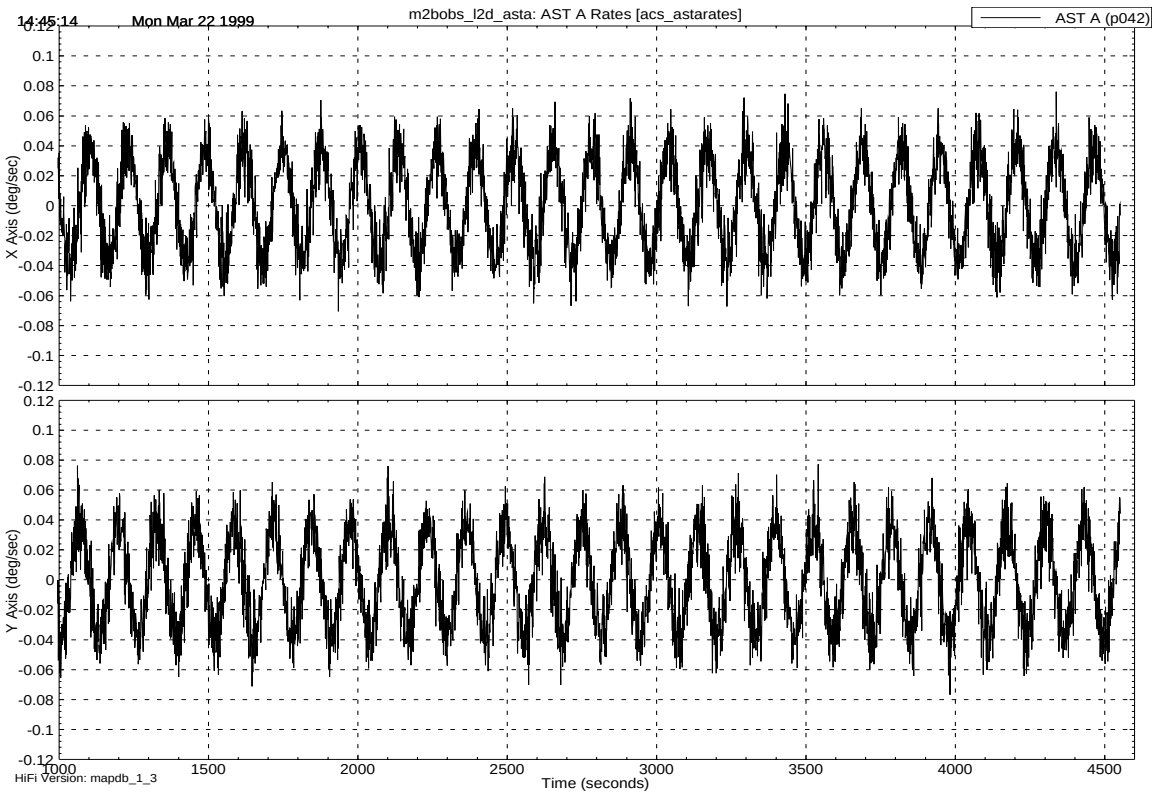

Figure 6: Star Tracker Derived Body Rates

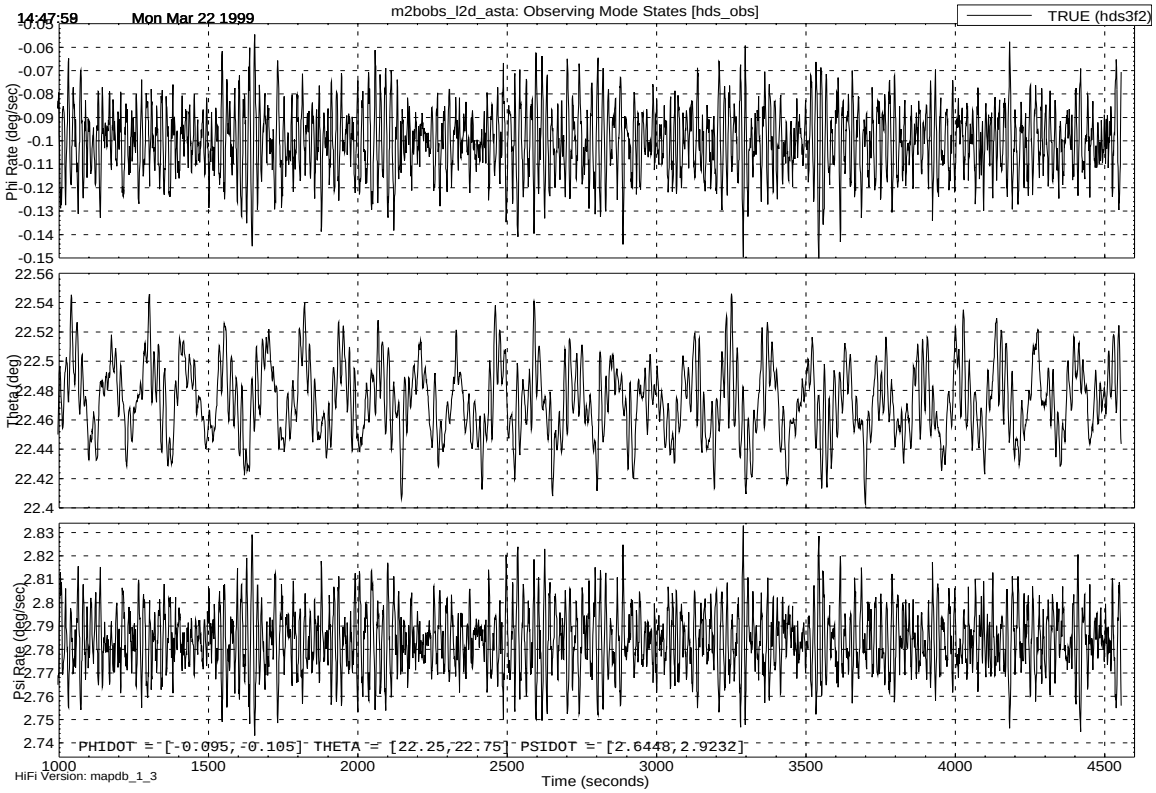

Figure 7: Observing Mode Performance Using Star Tracker Attitude and Derived Rate

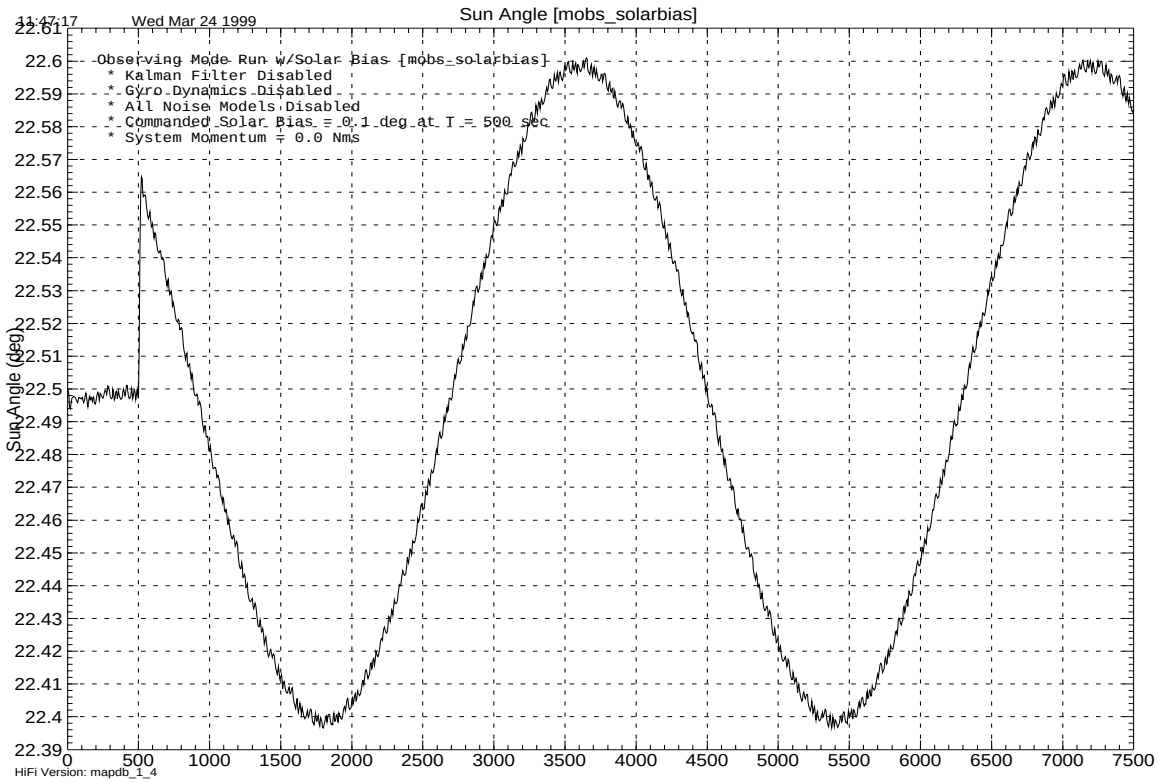

Figure 8: Sun Line Bias Angle

OTHER MAP BACKUP ALGORITHMS

In addition to the onboard backup algorithms implemented in the MAP flight software, a number of algorithms have been developed to cover other eventualities. These algorithms are not slated to be implemented on the spacecraft, either because of their complexity and impact that would have on the rest of the spacecraft flight software, or because the failure mode for which they were designed was considered relatively unlikely.

Observing Mode Thruster Unloading

As mentioned in the previous section, MAP is baselined to perform orbit and system momentum management operations four times a year. Using Tene's sun line bias, it might even be possible to reduce this number. However, due to a fairly large uncertainty about the rate of system momentum buildup, caused by a potential "pinwheel torque" on MAP (ref. 3), it may be necessary to use thrusters to dump momentum more often. In order to minimize the number of disruptions to science operations, an Observing Mode Thruster Unloading backup algorithm has been developed that: 1) unloads momentum to ≤ 0.3 Nms while in Observing Mode, 2) does not violate the 25° sun line constraint (violations of the $22.5 \pm 0.25°$ Observing Mode sun line angle constraint were permissible), and 3) can be completely executed during one ground pass of approximately 37.5 to 45 minutes.

Figure 9 shows a sketch of a “three shot” unloading process, which uses three thruster firings to unload system momentum. The steps in this process are as follows:

A. After the algorithm is enabled, wait until the transverse momentum is all in the +x axis. Fire thruster 2 to remove as much of this momentum as possible. This takes a maximum of one spin cycle (< 130 sec). [Coordinate system: X1,Z1]

B. After thruster firing A, wait until the sun is in the (–x,z) quadrant of the x-z plane. Fire thruster 1 or 2 (depending on the sign of the z-axis momentum) to add x-axis momentum equal to the amount of momentum in the z axis. This takes a maximum of one spin cycle (< 130 sec). [Coordinate system: X1,Z1] Note that this results in an intermediate system momentum state as much as $\sqrt{2}$ higher than the initial value. For a 1.5 Nms initial system momentum, this intermediate state could be as high as ~2.12 Nms. In simulation, this system momentum value does not pose an attitude control problem.

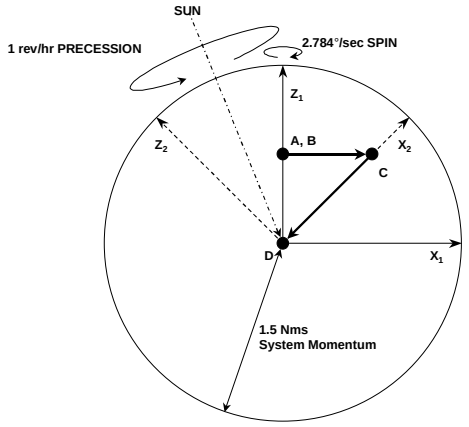

Figure 9: Unloading Schematic

C. After thruster firing B, wait approximately half of a precession cycle, and then wait until all of the system momentum is in the +x axis. Fire thruster 2 to remove as much of this momentum as possible. This takes a maximum of one half precession cycle plus one half spin cycle (< 1865 sec). [Coordinate system: X2,Z2]

D. After thruster firing C, a maximum of 35.5 minutes after the Observing Mode Thruster Unloading algorithm is enabled, system momentum is reduced close to zero. In simulation, it was found that the system momentum was reduced to less than 0.3 Nms for initial system momentum of 1.5 Nms.

Note that the algorithm as described uses thrusters 1 and 2. It could easily be adjusted to use only one of these two thrusters, or to use one of the other thruster pairs.

In simulation, this algorithm fulfills all of the previously stated requirements. Figure 10 shows the three thruster firings used in the example, one from thruster 1 and two from thruster 2. Figure 11 shows the resulting system momentum state of the spacecraft. Note that, after the first firing the system momentum is lower. The second firing, however, is used to align the system momentum vector so that, half a precession cycle later when the spacecraft has changed orientation by 45°, it will appear almost completely in the x-y plane. In this case, this caused a temporary increase in the system momentum of the spacecraft. The third firing reduces the system momentum to below 0.3 Nms. Figure 12 shows the Observing Mode performance during the operation of this algorithm. Other than the brief amount of time following each thruster firing, performance remains within requirements for the entire operation.

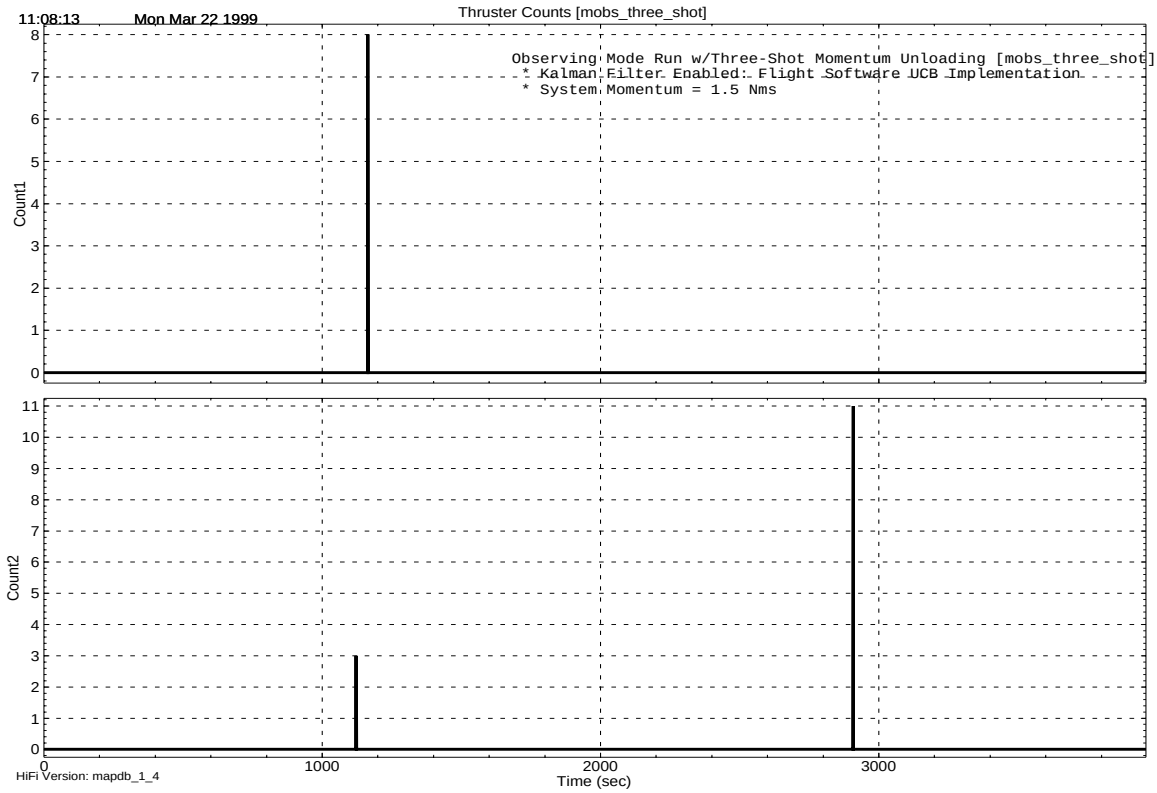

Figure 10: Observing Mode Thruster Unloading

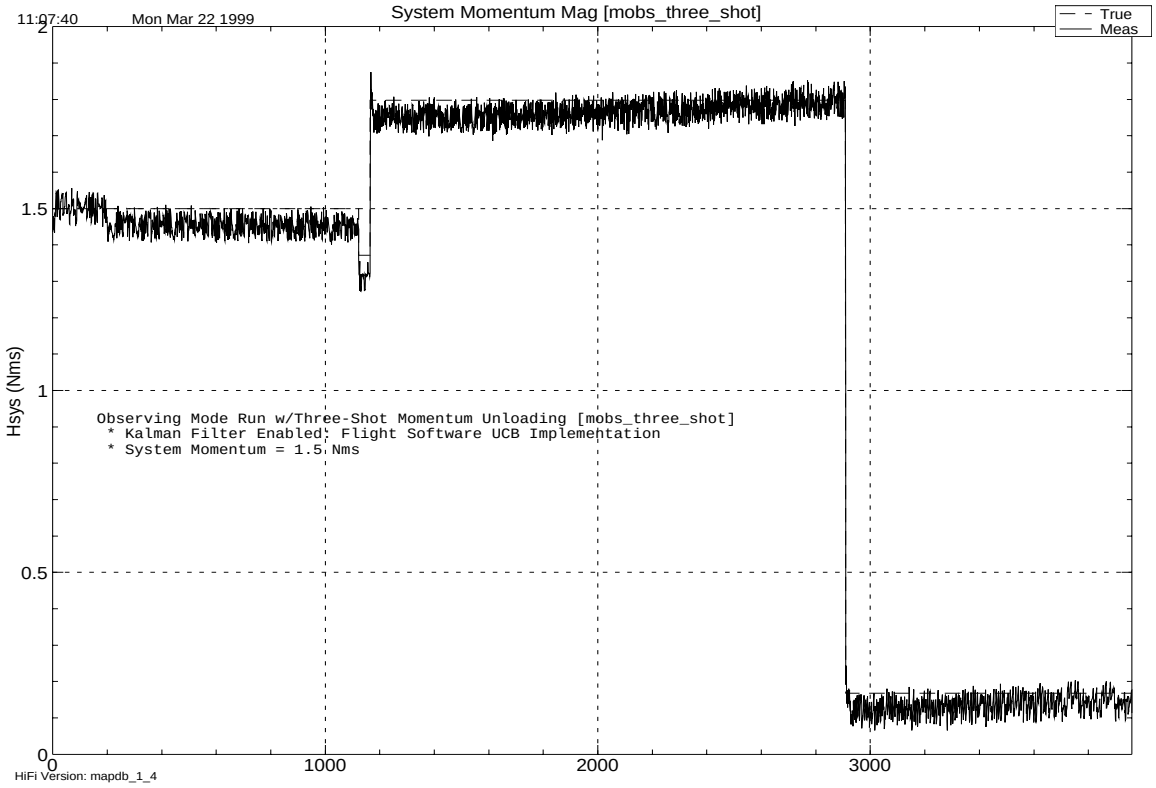

Figure 11: Observing Mode Thruster Unloading System Momentum

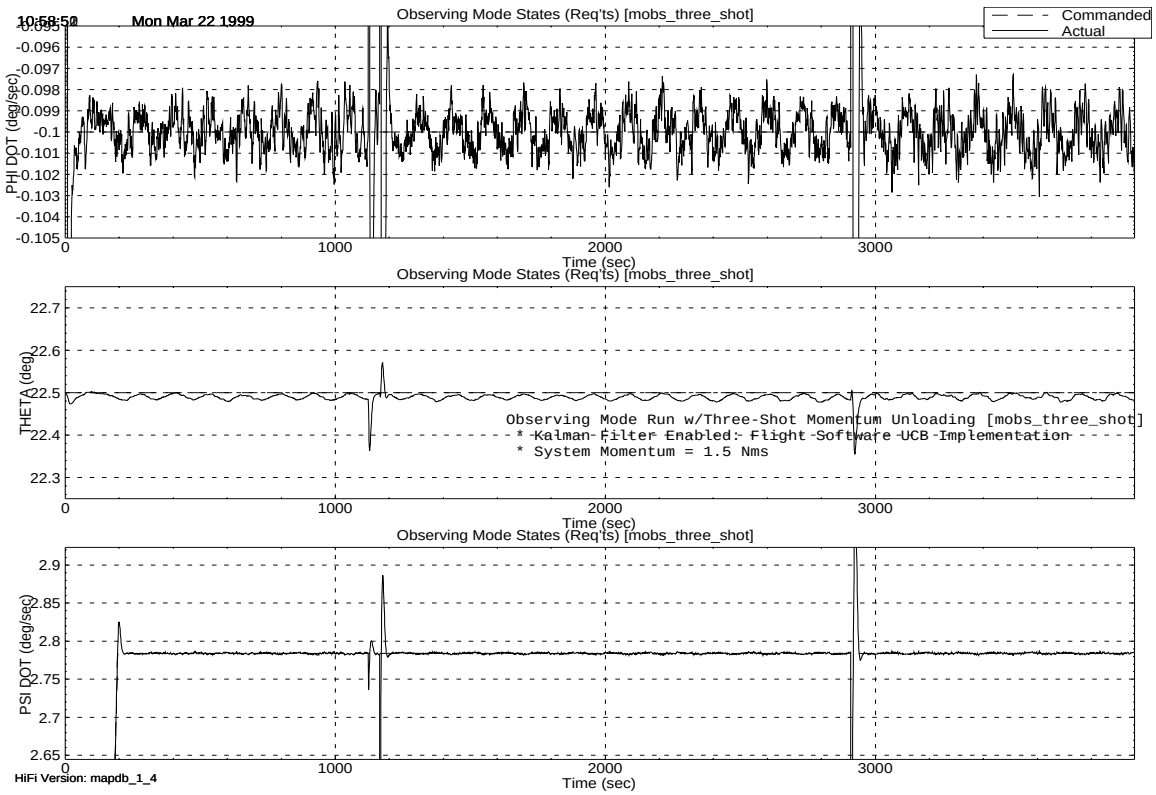

Figure 12: Observing Mode Performance During Thruster Unloading

Observing Mode Using One or Two Reaction Wheels

If one or two of the MAP reaction wheels were not available for control, the spacecraft could be spun up around the z-axis using thrusters. Then, using a single thruster in a pulsed mode (one pulse per spin period) the angular momentum vector could be moved into alignment with the sun vector with a simple spin-axis precession control law. During this maneuver, the spacecraft spin axis would continually nutate around the moving momentum vector. Each pulse would change the nutation (or cone) angle slightly, either increasing or decreasing it. The cone angle buildup would be well-bounded. In the vicinity of the target (the sun), a natural nutational instability would occur and would be taken advantage of. Once the sun is inside the nutation cone, each firing of the jet would increase the cone angle and disturb the angular momentum vector slightly in a pseudo-random direction. The basic motion would approximate a coning motion of the spin axis around the sun line with a continually-increasing nutation angle.

The nutation buildup would cease when the precession law is disabled. The spacecraft spin axis would then be coning around the sun line at some final cone angle. If this angle is 22.5°, the scan pattern produced for the sensors will cover the same region of space in the same amount of time as the normal mode controller, but the detailed motion will be significantly different (see Figure 13). The nominal controller provides a slow precession rate and fast spin rate. With the nutating single-spinner the precession rate is actually faster than the spin rate.

Since the spacecraft spin-axis is its maximum moment of inertia axis, the nutation angle will tend to decrease as a result of energy dissipation in the system. One reaction wheel could be used

to maintain the nutation angle at a desired magnitude with a simple control law. Since the sun will tend to drift away from the angular momentum vector, periodic jet firings would also be required to keep this deviation within acceptable limits.

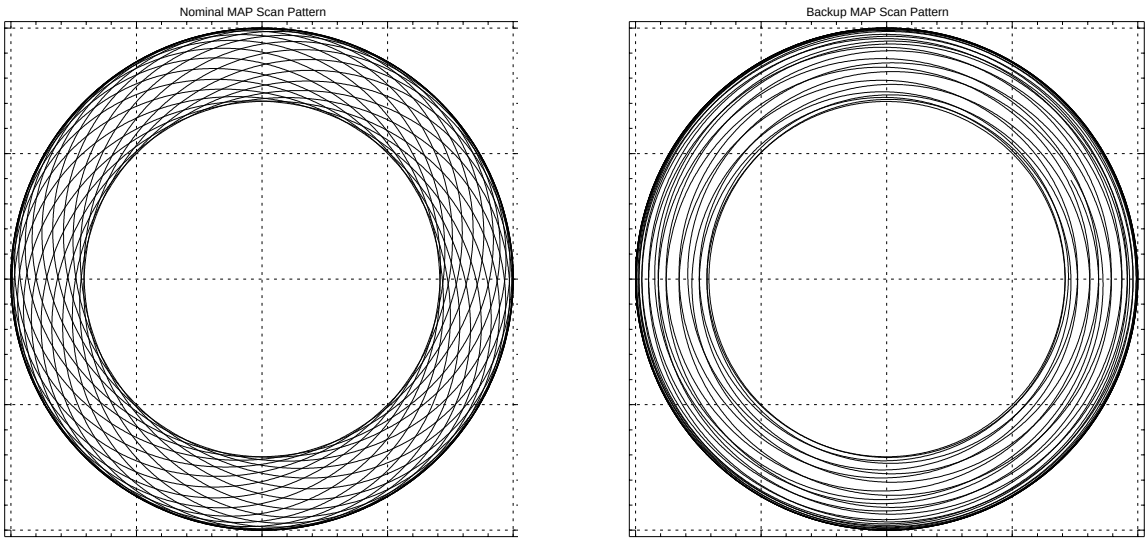

Figure 13: Nominal and Two-Wheel Backup Mode Scan Patterns

Figure 14 shows the sun angle in the body using this control algorithm. At 100 seconds, the spacecraft is spun up with a z-axis thruster firing. From 1000 to 3600 seconds, a single reaction wheel is used to control the nutation angle, bringing it to its steady state value by about 3200 seconds. Beginning at 3600 seconds, single-pulse thruster firings are used to align the spacecraft system momentum vector with the sun vector in the body frame. As described above, once the sun is within the nutation cone (after 4000 seconds in this example), further thruster firings disturb the system momentum vector in a pseudo-random direction and cause the nutation angle to increase. At 6000 seconds, the thruster firings are discontinued and the single-wheel nutation controller is enabled, used to minimize the nutation angle and keep the spacecraft precession cone angle within some tolerance of the desired value of 22.5°. (The residual nutation angle after the system has reached steady state is a result of the system momentum vector not being perfectly aligned with the sun vector.) After 8000 seconds, the spacecraft settles into the dual spin motion that will give the scan pattern shown in Figure 13.

CONCLUSION

In this paper, we have discussed how the MIDEX philosophy of “intelligent” redundancy was applied to the MAP spacecraft. The algorithms that have been designed for MAP, both those currently implemented in the spacecraft flight software and those held in reserve, allowed the project to modify the traditional full redundancy philosophy without a detrimental impact on the mission's probability of success. These algorithms allowed the project to focus its programmatic resources on other components that do not lend themselves to algorithmic workarounds, improving the reliability of the mission while maintaining the cost capped budget.

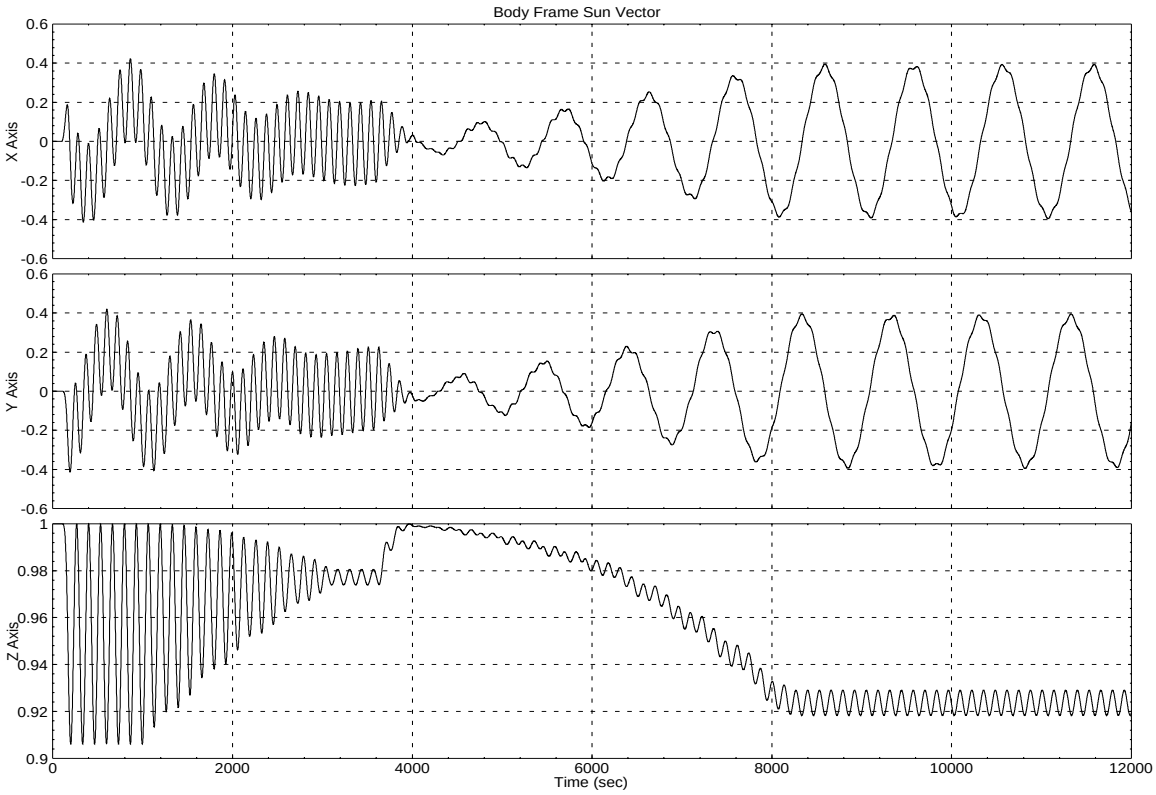

Figure 14: Two-Wheel Backup Mode Sun Vector in the Body Frame

DEDICATION

This paper is dedicated to our mentor and friend, Tom Flatley, who passed away in the past year. Thanks to Tom's intelligence, creativity, and perseverance, several missions have enjoyed extended lifetimes despite on-orbit failures by using algorithms similar to the ones described in this paper. Members of the space community will miss Tom's contributions to our profession through his simple, elegant designs, conceived within a mastery of flight dynamics. Members of the NASA Goddard community will also miss his quiet, unassuming dignity and warm, witty friendship.

REFERENCES

[1] Andrews, S., C. E. Campbell, A. J. Ericsson-Jackson, F. L. Markley, and J. R. O'Donnell, Jr., "MAP Attitude Control System Design and Analysis," *Flight Mechanics Symposium*, Goddard Space Flight Center, Greenbelt, MD, May, 1997.

[2] Ericsson-Jackson, A. J., S. F. Andrews, J. R. O'Donnell, Jr., and F. L. Markley, "MAP Stability, Design, and Analysis," *13th International Symposium on Space Flight Dynamics*, Goddard Space Flight Center, Greenbelt, MD, May, 1998.

[3] Tene, N., Karen Richon, David Folta, and Kimberly Tene, "Using Solar Radiation Pressure to Control L_2 Orbits," *13th International Symposium on Space Flight Dynamics*, Goddard Space Flight Center, Greenbelt, MD, May, 1998.